Supplementary information

Design, Synthesis and Characterization of Indolo[3,2-*a*]carbazole-Based Small Molecular Mass Organogelators as Hole Transporting Materials in Perovskite Solar Cell Applications

Jalaja Raghavan Haritha,[a] Nideesh Perumbalathodi,[b] Lincy Tom,[c] Kala Kannankutty,[b] Madambi Kunjukuttan Ezhuthachan Jayaraj,[d,e] Narayanapillai Manoj*,[a,e] Tzu-Chien Wei*,[b,f]

[a]*Department of Applied Chemistry Cochin University of Science and Technology, Kochi-22. E-mail: manoj.n@cusat.ac.in*

[b]*Department of Chemical Engineering National Tsing Hua University 101, Section 2, Kuang Fu Road, Hsinchu, Taiwan 30013, Republic of China*

[C]*Department of Chemistry, Nirmala College, Muvattupuzha, 686661, Ernakulam, Kerala.*

[d]*University of Calicut, Thenhipalam, Malappuram, Kerala, 673635*

[e]*Centre of Excellence in Advanced Materials, Cochin University of Science and Technology, Kochi-22*

[f]*Center for Emergent Functional Matter Science, National Yang Ming Chiao Tung University, Hsinchu 300093, Taiwan. Email tcwei@mx.nthu.edu.tw*

E-mail: *manoj.n@cusat.ac.in*

Table of Contents

1. General Techniques

All the analytical grade chemical reagents and solvents are purchased from commercial sources and used them without any further purification. For photophysical studies, we employed Spectroscopic grade solvents from Merck. The melting point was determined using a JSGW melting point apparatus. The ^{1}H and ^{13}C NMR spectra were recorded on a Bruker Avance III FT-NMR spectrometer at 400 and 100 MHz, respectively. Deuterated chloroform ($CDCl_3$) served as the solvent, with tetramethylsilane (TMS) as the internal standard. The MALDI-TOF mass spectrum was obtained using a Bruker Autoflex max LRF. UV-Visible absorption spectra were recorded at room temperature using an Evolution 201 UV–vis spectrophotometer. Fluorescence emission spectra measurements were taken at room temperature on a Horiba Fluorolog 3 spectrofluorimeter, with both the excitation and emission slit widths set to 2 nm. Thermogravimetric analysis (TGA) was performed using a Perkin Elmer Pyris Daimond TG/DTG instrument under nitrogen as the carrier gas. Thermal behavior including phase transitions and melting properties (melting and glass transition temperatures) were measured in a heat flux differential scanning calorimeter (Netzsch DSC 204 F1 Heat flux DSC) using hermetically sealed aluminum crucibles (25 µL), at heating rate of 20 $^{o}C\ min^{-1}$ and under constant flow (50 $cm^3\ min^{-1}$) of nitrogen (N_2). Cyclic voltammetry experiments were carried out using a CHI660E Electrochemical Workstation. The CV data were analysed with a conventional three-electrode system comprising a platinum disk as the working electrode, platinum wire as the auxiliary electrode, nonaqueous Ag electrode as the reference electrode and 0.1 M tetrabutylammonium hexafluorophosphate (TBAPF6) as the supporting electrolyte. The electrochemical potentials for the synthesized molecules were calibrated against an Fc/Fc+ internal standard at 0.64 V. DFT analysis were done using Gaussian 09 software with B3LYP exchange correlation energy functional and 6-311 G (d, p) basis set. The electronic transitions and their oscillator strengths were determined by the TD-DFT method using the same functional and basis set. The optimized geometry and the respective electronic transitions in different solvents were obtained using the polarizable continuum model CPCM, as implemented in Gaussian 09. Crystallographic data were collected with a Bruker SMART APEX diffractometer with graphite monochromated Mo Kα (λ = 0.71073 Å) X-ray source. Bruker SMART software was used for data acquisition and Bruker

SAINT Software for data integration. Absorption corrections were carried out using SADABS based on Laue symmetry using equivalent reflections. The structure was solved by direct methods using the SHELXL-97 software package and refined on F by full matrix least squares. All the drawings of compounds were made using DIAMOND 3.2 and MERCURY 3.8 programs. The X-ray diffraction (XRD) spectra of powder and thin film samples of C_RISc were explored in a high-resolution Bruker D8 Advance Twin- Twin diffractometer.Water contact angle for the synthesised molecules were measured using Rame-heart Goniometer. The topography of different gel samples was characterized by field-emission scanning electron microscopy (FESEM, Carl Zeiss – Sigma, SMARTSEM software), and surface roughness was evaluated by atomic force microscopy (AFM, C3000, Nanosurf, Switzerland). Transmittance spectra were recorded by HITACHI-U-3900 Spectrometer (Japan). Optical microscopic images are taken by OLYMPUS-BX5Mtr (Japan).

2. Experimental Procedures

Synthesis of 5,12-Dialkyl-6,7-Diphenyl-5,12-Dihydroindolo[3,2 *a*]Carbazole (1-6)

The general method for the synthesis of 5,12-dialkyl-6,7-diphenyl-5,12-dihydroindolo[3,2 *a*]carbazole derivatives **(1-6)** is according to previously reported synthetic procedures.[1] The reaction involves condensation reaction between N-alkylindole and benzyl in presence of *p*-toluenesulfonic acid (20 mol%) in dry toluene. The product obtained as a colourless crystalline solid with ~75% yield, after the solvent was removed *in vacuo* and the residue was purified by silica gel column chromatography (60–120 mesh, hexane–ethyl acetate solvent mixture) which was characterized as the indolo[3,2-*a*]carbazole.

3. Results and Discussions

Characterization: **Compound 1.** 5,12-dibutyl-6,7-diphenyl-5,12-dihydroindolo[3,2-*a*] carbazole (C_4IC)

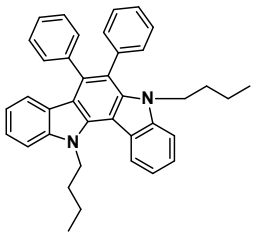

Chemical formula: $C_{38}H_{36}N_2$

Yield: 77 %

m.p: 167 ^oC

Appearance: Colourless Solid

IR(KBr): $\nu_{max}(cm^{-1})$ = 3005 (C-H), 1505 (C=C), 1356 (C-N).**^{1}H NMR** (400 MHz, $CDCl_3$, δ ppm): 8.44 (d, 1H, *J* = 8Hz), 7.46 (quint, 3H, *J* = 8Hz), 7.31-7.18 (m, 11H), 6.86 (t, 1H, *J* = 8Hz), 6.43 (d, 1H, *J* = 8Hz), 4.93 (d, 2H, *J* = 8Hz), 3.71 (t, 2H, *J* = 8Hz), 2.21 (quint, 2H, *J* = 7.8Hz), 1.62-1.45 (m, 4H), 1.43-1.03 (m, 3H), 0.84 (t, 2H, *J* = 8Hz), 0.71 (t, 3H, *J* = 8Hz). **^{13}C NMR** (100 MHz, $CDCl_3$, δ ppm): 141.2, 141.0, 140.3, 138.8, 138.3, 135.9, 131.9, 130.4, 127.8, 127.3, 126.6, 126.5, 124.5, 124.1, 123.5, 122.4, 121.2, 119.1 (2C), 118.2, 115.1, 109.5, 109.0, 107.4, 46.3, 44.4, 33.0, 30.8, 20.2, 19.8, 14.0, 13.6. **MALDI- TOF MS** (ESI MS) m/z: $[M+H]^+$ calcd for $C_{38}H_{36}N_2$:521.2957, found :521.6194.

Compound 2. 5,12-dioctyl-6,7-diphenyl-5,12-dihydroindolo[3,2-*a*] carbazole (C_8IC)

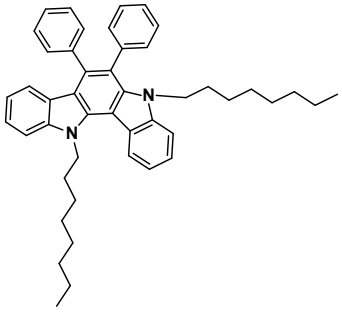

Chemical formula: $C_{46}H_{52}N_2$

Yield: 78 %

m.p: 92 ^oC

Appearance: Colourless Solid

IR (KBr): ν_{max} (cm^{-1}) = 2995 (C-H), 1499 (C=C), 1358 (C-N). **^{1}H NMR** (400 MHz, $CDCl_3$, δ ppm): 8.34 (d, 1H, *J* = 8.4Hz), 7.41-7.10 (m, 15H), 6.78 (s, 1H), 6.35 (d, 1H, *J* = 8Hz), 4.82 (t, 2H, *J* = 8.2Hz), 3.62 (t, 2H, *J* = 8.2Hz), 2.14 (s, 2H), 1.50-0.99 (m, 28H), 0.82-0.71 (m, 2H). **^{13}C NMR** (100 MHz, $CDCl_3$, δ ppm): 141.2, 140.9, 140.3, 138.9, 138.3, 136.2, 135.9, 131.9, 130.4, 127.8, 127.3, 126.6, 126.5, 124.5, 124.1, 123.5, 122.4, 121.2, 119.1 (2C), 118.2, 115.1, 109.5, 109.0, 107.4, 46.5, 44.6, 31.8, 31.7, 30.9, 29.4, 29.2,

29.1 (2C), 28.7. 26.9, 26.6, 22.6 (2C). **MALDI- TOF MS** (ESI MS) m/z: $[M+H]^+$ calculated for $C_{45}H_{50}N_2$633.4203, found 633.2945.

Compound 3. 5,12-didodecyl-6,7-diphenyl-5,12-dihydroindolo[3,2-*a*]carbazole (C_{12}IC)

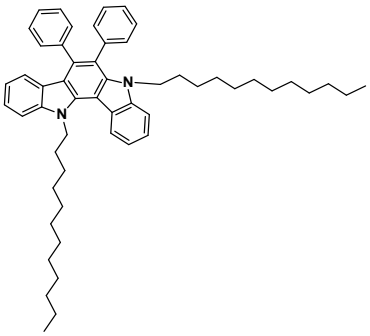

Chemical formula: $C_{54}H_{68}N_2$

Yield: 78 %

m.p: 77 ^oC

Appearance: Colourless Solid

IR (KBr): ν_{max} (cm^{-1}) = 2923 (C-H), 1630 (C=C), 1117 (C-N). **^{1}H NMR** (400 MHz, $CDCl_3$, δ ppm): 8.34 (d, 1H, *J* = 8 Hz), 7.40-7.33 (m, 3H), 7.24-7.16 (m, 7H), 7.12-7.09 (m, 5H), 6.77 (t, 1H, *J* = 7.6 Hz), 6.35 (d, 1H, *J* = 8 Hz), 4.81 (t, 2H, *J* = 8 Hz), 3.61 (t, 2H, *J* = 8 Hz), 1.4 (t, 2H, *J* = 7.2 Hz), 1.5 (d, 2H, *J* = 7.2 Hz), 1.39-1.35 (m, 5H), 1.08-0.98 (m, 4H), 0.79-0.78 (m, 6H), 0.70 (t, 2H, *J* = 7 Hz). **^{13}C NMR** (100 MHz, $CDCl_3$, δ ppm): 140.1, 139.9, 138.0, 137.0, 136.6, 135.4, 133.2, 132.3, 131.0, 130.2, 129.7, 123.4, 123.0, 122.8, 121.4, 120.1, 120.0, 119.9, 118.3, 115.5, 113.8, 108.6, 108.1, 106.7, 45.5, 43.7, 30.7 (2C), 29.8, 28.3, 28.1 (3C), 27.7, 25.8, 25.6, 21.6, 13.0. **MALDI- TOF MS** (ESI MS) m/z: $[M+H]^+$ calculated for $C_{54}H_{68}N_2$745.5461, found 745.7536.

Compound 4. 5,12-dihexadecyl-6,7-diphenyl-5,12-dihydroindolo[3,2-*a*]carbazole (C_{16}IC)

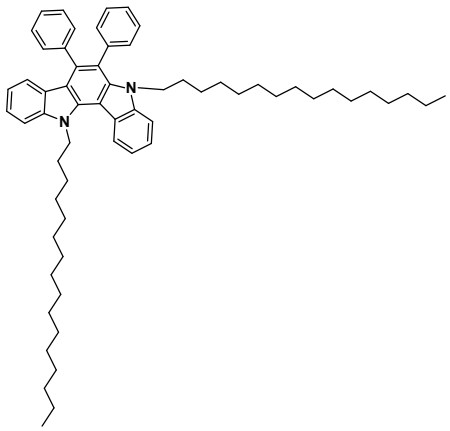

Chemical formula: $C_{62}H_{84}N_2$

Yield: 78 %

m.p: 72 ^oC

Appearance: Colourless Solid

IR (KBr): ν_{max} (cm^{-1}) = 2923 (C-H), 1632 (C=C), 1119 (C-N). **^{1}H NMR** (400 MHz, $CDCl_3$, δ ppm): 8.36 (d, 1H, *J* = 8.4 Hz), 7.43 (s, 1H), 7.41-7.39 (m, 1H), 7.38-7.35 (m, 1H), 7.26-7.21 (m, 3H), 7.20-7.19 (m, 4H), 7.18-7.12 (m, 5H), 6.79 (t, 1H, *J* = 7.6 Hz), 6.36 (d, 1H, *J* = 8 Hz), 4.84 (t, 2H, J = 8.2 Hz), 3.63 (t, 2H, *J* = 8.2 Hz), 2.16 (quint, 2H, *J* = 7.8 Hz), 1.52 (q, 2H, *J* = 7.8 Hz), 1.52 (q, 2H, *J* = 7.3 Hz), 1.35 (q, 4H, *J* = 6.5 Hz), 1.22-1.09 (m, 46H), 0.82-0.78 (m, 6H), 0.72 (q, 2H, *J* = 7.3). **^{13}C NMR** (100 MHz, $CDCl_3$, δ ppm): 140.0, 139.8, 139.3, 137.8, 137.2, 135.2, 134.9, 130.8, 129.3, 126.8, 126.3, 125.6, 125.5, 123.4, 123.1, 122.5, 121.3, 120.1, 118.0, 117.1, 114.0, 108.4, 107.9, 106.3, 45.5, 43.6, 30.9, 28.6, 28.5 (2C), 28.4, 28.3, 21.6, 13.1. **MALDI- TOF MS** (ESI MS) m/z: $[M+H]^+$ calculated for $C_{62}H_{84}N_2$ 857.6713, found 857.8620.

Compound 5. 5,12-dioctadecyl-6,7-diphenyl-5,12-dihydroindolo[3,2-*a*]carbazole (C_{18}IC)

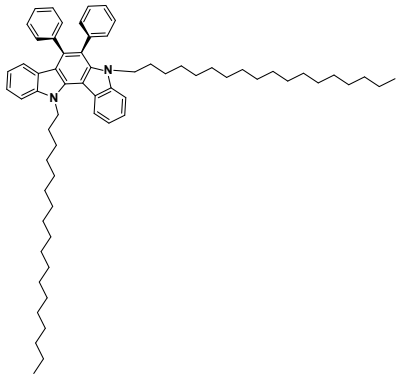

Chemical formula: $C_{66}H_{92}N_2$

Yield: 78 %

m.p: 76 ^oC

Appearance: Colourless Solid

IR (KBr): ν_{max} (cm^{-1}) = 2928 (C-H), 1632 (C=C), 1117 (C-N). **^{1}H NMR** (400 MHz, $CDCl_3$, δ ppm): 8.36 (d, 1H, *J* = 8Hz), 7.45 – 7.35 (m, 3H), 7.26 – 7.17 (m, 8Hz), 7.15 – 7.12 (m, 4H), 6.79 (t, 1H, *J* = 7.6Hz), 6.36 (d, 1H, *J* = 7.6), 4.84 (t, 2H, *J* = 8Hz), 3.63 (t, 2H, *J* = 8.2Hz), 2.16 (quint, 2H, *J* = 7.8Hz), 1.53-1.49 (m, 2H), 1.35 (t, 4H, *J* = =7.6Hz), 1.22-1.00 (m, 54H), 0.82-0.78 (m, 6H), 0.72 (t, 2H, *J* = 7Hz). **^{13}C NMR** (100 MHz, $CDCl_3$, δ ppm):

140.1, 139.8, 139.3, 137.8, 137.2, 135.2, 134.9, 130.8, 129.3, 126.8, 126.3, 125.6, 125.5, 123.4, 123.1, 122.5, 121.3, 120.1, 180.0 (2C), 117.1, 114.0, 108.4, 107.9, 106.3, 66.9, 45.5, 43.6, 30.9, 28.6 (2C), 28.5 (2C), 28.4, 28.3, 21.6, 13.1. **MALDI- TOF MS** (ESI MS) m/z: $[M+H]^+$ calculated for $C_{66}H_{92}N_2$ 913.7339, found 913.9362.

Compound 6. 5,12-bis(2-ethylhexyl)-6,7-diphenyl-5,12-dihydroindolo[3,2-*a*]carbazole (C_{ex}IC)

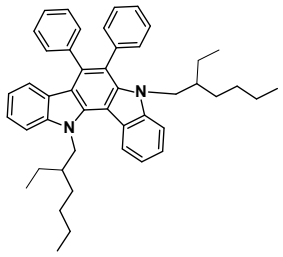

Chemical formula: $C_{46}H_{52}N_2$

Yield: 78 %

m.p: 142 ^oC

Appearance: Colourless Solid

IR (KBr): ν_{max} (cm^{-1}) = 2965 (C-H), 1571 (C=C), 1470 (C-N). **^{1}H NMR** (500 MHz, $CDCl_3$, δ ppm): 8.43 (d, 1H, *J* = 8Hz), 7.50-7.43 (m, 3H), 7.32-7.16 (m, 12H), 6.85 (t, 1H, *J* = 7Hz), 6.46 (d, 1H, *J*=7.5Hz), 4.93 (d, 2H, *J* = 7Hz), 3.71 (d, 2H, *J* = 5.5Hz), 2.15 (s, 1H), 1.69 (s, 1H), 1.48 (s, 1H), 1.08-0.95 (m, 8H), 0.81 (s, 3H), 0.66 (t, 10H, *J* = 8Hz), 0.52 (t, 6H, *J* = 6.3Hz). **^{13}C NMR** (125 MHz, $CDCl_3$, δ ppm): 141.7, 140.5, 139.1 (2C), 138.8, 136.7, 135.8, 132.5, 130.5, 127.8 (2C), 127.3, 126.5, 126.4, 125.1, 123.2, 123.1, 121.2, 121.1, 119.1, 118.8, 118.7, 115.6, 110.4, 108.2, 50.2, 48.2, 38.8, 38.5, 29.7 (2C), 29.6 (2C), 28.1 (2C), 28.0, 23.3, 23.0, 22.9, 22.7, 13.8, 13.7, 10.5, 10.4. **MALDI- TOF MS** (ESI MS) m/z: $[M+H]^+$ calculated for $C_{45}H_{50}N_2$ 633.4209, found 633.3700.

4. Supporting Schemes, Figures and Tables

4.1. Single crystal analysis of C_RIC HTMs

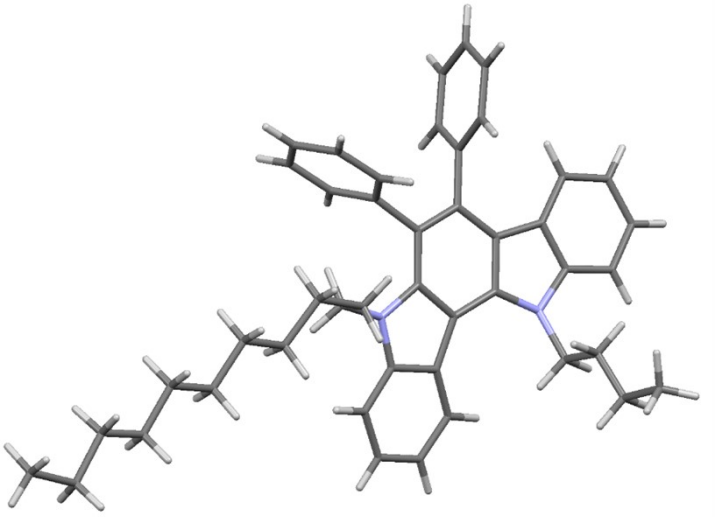

Figure S1. Partially solved structure of C_{12}IC.

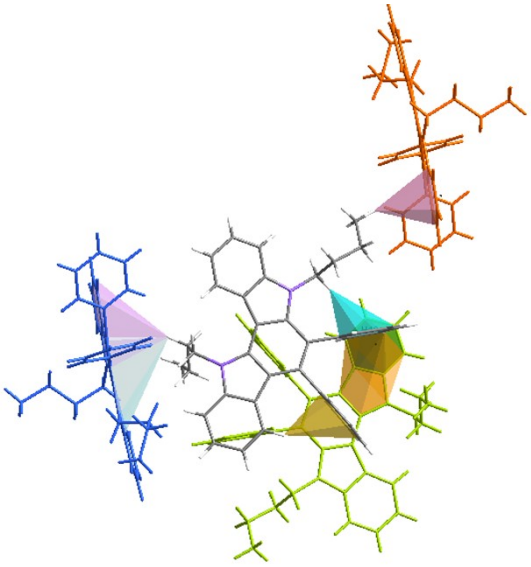

Figure S2. Intramolecular and intermolecular C–H···π interactions in C_4IC.

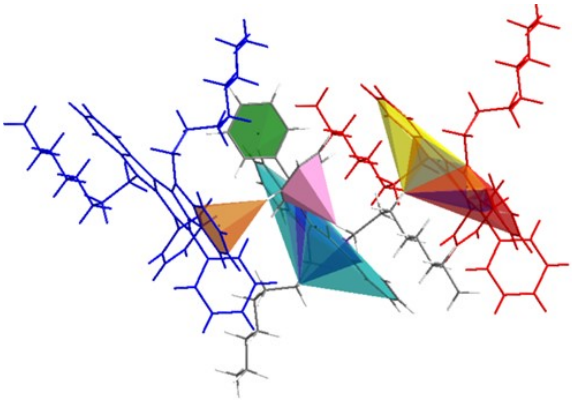

Figure S3. Intramolecular and intermolecular C–H···π interactions in C_8IC.

Table S1. Crystal data and structure refinement summary for C_4IC and C_8IC

Empirical formula	$C_{38}H_{36}N_2$	$C_{46}H_{52}N_2$
Formula weight	520.69	632.90
Temperature	296(2) K	296(2) K
Wavelength	0.71073 Å	0.71073 Å
Space group	P 21/n	P-1
Unit cell dimensions	a = 12.8861(13) Å α= 90°. b = 11.8091(12) Å β= 90°. c = 19.104(2) Å γ = 120°.	a = 12.9436(9) Å α= 90°. b = 12.9490(10) Å β= 90°. c = 13.5857(10) Å γ = 120°.
Volume	2890.1(5) $Å^3$	1855.8(2) $Å^3$
Z	4	2
Density (calculated)	4 Mg/m^3	1.133 Mg/m3
Absorption coefficient	0.069 mm^{-1}	0.065 mm^{-1}
F(000)	1112	684
Reflections collected	31322	15570
Independent reflections	7243 [R(int) = 0.0393]	8256 [R(int) = 0.0304]
Goodness-of-fit on F^2	0.973	1.034
Data / restraints / parameters	7243 / 0 / 363	8256 / 0 / 436
Final R indices [I>2sigma(I)]	R_1 = 0.0679, wR_2 = 0.2104	R1 = 0.0885, wR2 = 0.2501

C-H···Cg (Å)	H···Cg (Å)	C-H···Cg (°)
C9-H9B···Cg(5)[a]	2.79	45
C12-H12C···Cg(7)[b]	2.88	69
C16-H16···Cg(7)[c]	2.69	63
C16-H16···Cg(11)[c]	2.93	63
C30-H30B···Cg(14)[d]	2.99	56
C30-H30B···Cg(16)[d]	2.94	55
C34-H34···Cg(6)[a]	2.84	35

Table S2. C–H···π interactions in C_4IC

Symmetry code a= x,y,z, b=-1/2+x,1/2-y,1/2+z, c= 1-x,1-y,1-z, d=1/2-x,1/2+y,1/2-z

Cg(5) - C14,C15,C16,C17,C18, C19

Cg(6) - C21,C22,C23,C24,C25,C26

Cg(7) - C33,C34,C35,C36,C37, C38

Cg(11) - N2,C28,C27,C33,C34,C35,C36,C37,C38

Cg(14) - N2,C28,C7,C8,C13,C20,C27,C33,C34,C35,C36,C37,C38

Cg(16) - N1,C5,C6,C7,C28,N2,C38,C37,C36,C35,C34,C33,C27,C20,C13,C8

Table S3. C–H···π interactions in C_8IC

C-H···Cg (Å)	H···Cg (Å)	C-H···Cg (°)
C7-H7B···Cg(15)[a]	2.84	1
C7-H7B···Cg(17) [a]	2.75	0
C10-H10···Cg(6) [a]	2.79	38
C26-H26A···Cg(7)[a]	2.67	44
C28-H28A···Cg(12)[b]	2.90	66
C28-H28A ···Cg(15)[b]	2.72	69
C28-H28A ···Cg(17)[b]	2.59	69
C45-H45···Cg(3)[c]	2.82	64

Symmetry code a= x,y,z, b=1-x,-y,-z, c=2-x,-y,-z

Cg(15) - N1,C14,C9,C16,C34,C17,C18,N2,C25,C24,C23,C22,C21,C20,C19,C15

Cg (17) -

N1,C14,C13,C12,C11,C10,C9,C16,C34,C17,C18,N2,C25,C24,C23,C22,C21,C20,C19,C15

Cg(6) - C35,C36,C37,C38,C39,C40

Cg(7) - C41,C42,C43,C44,C45,C46

Cg (12) - N1,C14,C9,C16,C34,C17,C18,N2,C25,C20,C19,C15

Cg (15) - N1,C14,C9,C16,C34,C17,C18,N2,C25,C24,C23,C22,C21,C20,C19,C15

Cg(17) -

N1,C14,C13,C12,C11,C10,C9,C16,C34,C17,C18,N2,C25,C24,C23,C22,C21,C20,C19,C15

Cg(3) - C9,C10,C11,C12,C13,C14

4.2. Theoretical calculations of C_RICs

Table S4. Calculated dihedral angles (°) of indolocarbazole derivatives after geometry optimization.

C_RICs	Dihedral angles (°) ($G\phi_1$= C_{13}-C_{14}-C_{27}-C_{28})	Dihedral angles (°) ($G\phi_{2=}$ C_{40}-C_{38}-C_{15}-C_{16})
C_1IC	71	81
C_4IC	82	90
C_{12}IC	81	84

Table S5. Theoretical and experimental values of all the energy levels in C_RIC HTMs.

HTMs	[a] E_{HOMO} (eV)	[b] E_{LUMO} (eV)	[c] HOMO (IP)/eV	[d] LUMO (EA)/eV vacuum	[e] λ_{abs} (nm)	[f] λ_{emi} (nm)	[g] $E_{0\text{-}0}$ (eV)
C_4IC	-5.15	-0.96	-5.39	-2.13	369	392	3.26
C_8IC	-5.16	-0.98	-5.40	-2.14	370	394	3.26
C_{12}IC	-5.16	-0.98	-5.41	-2.15	370	393	3.26
C_{ex}IC	-5.16	-1.01	5.40	-2.11	370	387	3.29

[a]E_{HOMO}, [b]E_{LUMO} is obtained from DFT calculation using 6311g (d,p) as the basis set. The oxidative onset potential (E_{ox} vs Fe/Fe^+) was measured by CV in acetonitrile. [c] HOMO = -[4.8 + (E_{ox} – Fe/Fe^+)] [d] E_{LUMO} = H_{OMO} – $E_{0\text{-}0}$. [e] UV-visible absorption was measured in THF with a concentration of 10^{-5} M. [f] Photo-luminescent data were recorded in 10^{-5} M solutions in THF. [g] Energy gap calculated from the insertion of absorption and emission maxima.

4.3. Photophysical characterisation of C_RICs

Table S6. Photophysical characterisation data of C_RICs.

C_RICs	λ_{abs} (nm)	λ_{emi} (nm)	E_{0-0} Optical (eV)
C_4IC	369	392	3.26
C_8IC	370	394	3.26
C_{12}IC	370	393	3.26
C_{16}IC	370	387	3.29
C_{18}IC	370	386	3.30
C_{ex}IC	370	387	3.29
Spiro-OMeTAD	386	416	3.06

4.4. Intersection of UV-Vis absorption and fluorescence emission spectra of C_RICs

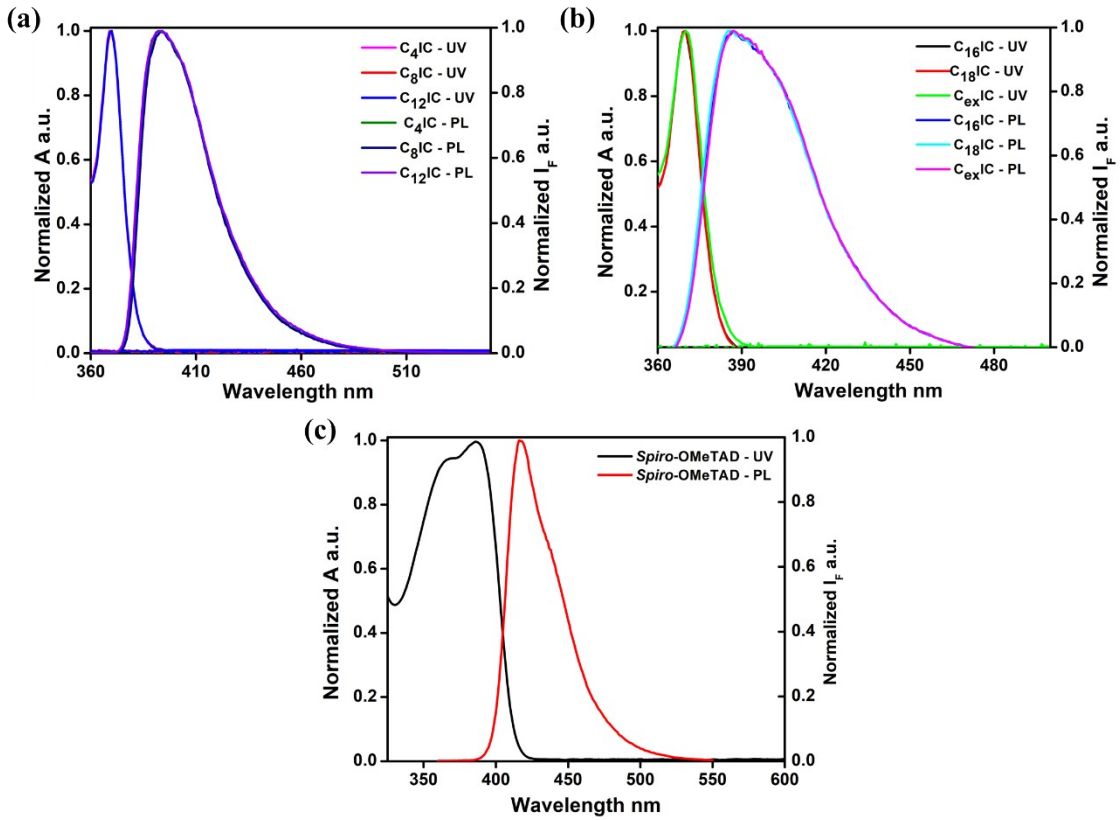

Figure S4. Intersection of UV-Vis absorption and fluorescence emission spectra of C_RICs (a), (b) and *Spiro*-OMeTAD (c) recorded in 10^{-5} M THF solution

4.5. Electrochemical characterisation of C_RICs

Table S7. Electrochemical data of C_RICs in acetonitrile

HTM	[a] E_{ox} vs Fe/Fe+ (V)	[b] HOMO (IP)/eV	[c] LUMO (EA)/eV vacuum	[d] E_{0-0} (eV)
C_4IC	0.60	-5.40	-2.14	3.26
C_8IC	0.61	-5.41	-2.15	3.26
C_{12}IC	0.61	-5.41	-2.15	3.26
C_{16}IC	0.60	-5.40	-2.11	3.29
C_{18}IC	0.61	-5.41	-2.11	3.30
C_{ex}IC	0.61	-5.41	-2.12	3.29
Spiro-OMeTAD	0.56	-5.36	-2.30	3.06

[a] The oxidative onset potential (E_{ox} vs Fe/Fe^+) was measured by CV in acetonitrile. [b] HOMO = -[4.8 + (E_{ox} – Fe/Fe^+)]. [c] Energy gap (E_{0-0}) calculated from the insertion of absorption and emission maxima which were recorded in 10^{-5} M solutions in THF. [d] $E_{LUMO} = H_{OMO} – E_{0-0}$.

4.6. Thermal characterisation of C_RICs

Table S8. Thermal properties of C_RICs and *Spiro*-OMeTAD.

C_RICs	C_4IC	C_8IC	C_{12}IC	C_{16}IC	C_{18}IC	C_{ex}IC	*Spiro*-OMeTAD[2]
T_d [°C]	356	398	419	440	443	363	449

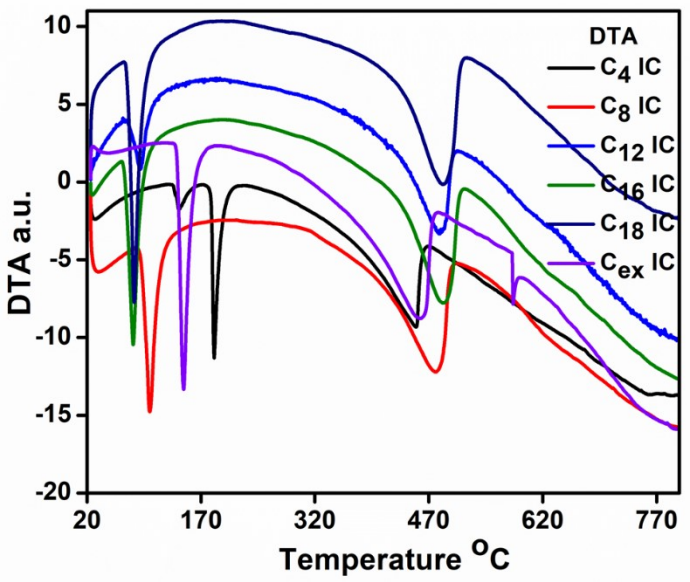

Figure S5. DTA analysis of HTMs under nitrogen (scan rate 10^{o}C min^{1}) atmosphere.

4.7. Gelation properties of C_RICs

Table S9. Gelation abilities of compounds **1-6** in organic solvents

Sl No:	**Solvents**	C_4IC	C_8IC	C_{12}IC **CGC/mmol**	C_{16}IC	C_{18}IC	C_{ex}IC
1	Water	P	P	P	P	P	P
2	Acetonitrile	P	P	P	P	P	P
3	Acetone	P	P	P	P	P	P
4	Methanol	P	P	P	P	P	P
5	THF	S	PG	G (1.1)	P	PG	PG
6	Propanol	P	P	P	P	P	P

7	DCM	S	S	S	S	S	S
8	Chloroform	S	S	S	S	S	S
9	Toluene	S	PG	G (1.4)	P	PG	PG
10	Hexane	P	P	P	P	P	P
11	DMSO	S	S	S	S	S	S
12	DMF	S	S	S	S	S	S
13	Propanol- DCM	S	S	G (3.2)	S	S	S
14	THF-Water	P	P	G (1.1)	P	P	P
15	Hexane-Water	P	PG	G (2.6)	P	P	P
16	DCM-Water	P	P	G (2.8)	P	P	P
17	Hexane - DCM	P	P	G (2.4)	P	P	P

P= precipitate; PG = partly gel; S = soluble; G = gel; CGC: critical gelation concentration

4.8. Thin film forming properties of C_RICs

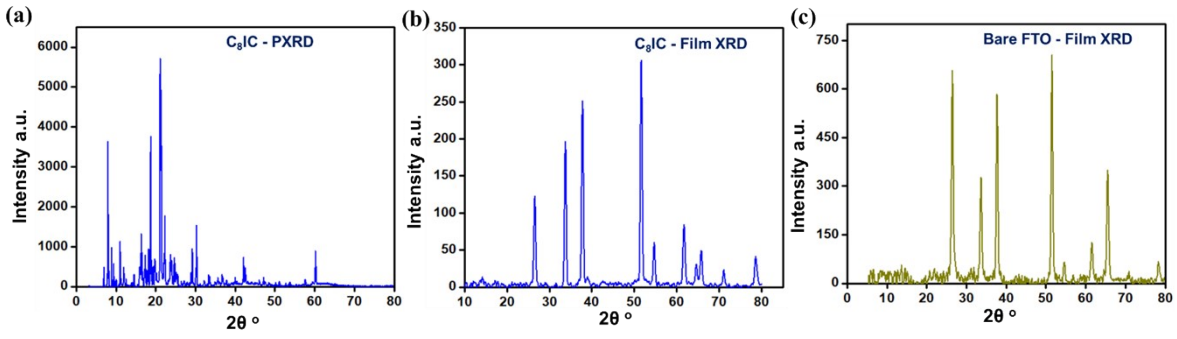

Figure S6. X-ray diffraction patterns of powder samples of **(a).**C_8IC and thin film samples of **(b).** C_8IC on FTO substrate. **(d).** PXRD spectrum of bare FTO substrate

4.9. Optical microscopic images of C_RICs and *Spiro*-OMeTAD films on FTO and PVSK

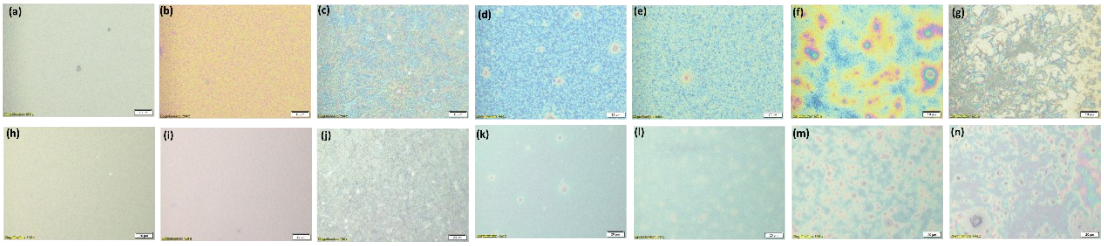

Figure S7. Optical microscopic images of C_RICs and *Spiro*-OMeTAD films on FTO and PVSK film **(a).** bare FTO**, (b).** FTO/spiro-OMeTAD **(c).** FTO/C_4IC**, (d).** FTO/C_8IC**, (e).** FTO/C_{12}IC, **(f).** FTO/C_{16}IC**, (g).** FTO/C_{18}IC**, (h).** glass/PVSK**, (i).** glass/PVSK/spiro-OMeTAD **(j).** glass/PVSK/C_4IC**, (k).** FTO/PVSK/C_8IC**, (l**). FTO/PVSK/C_{12}IC, **(m).** glass/PVSK/C_{16}IC**, (n).** glass/ PVSK/C_{18}IC.

4.10. Transmittance spectra of C_RIC films on FTO substrate

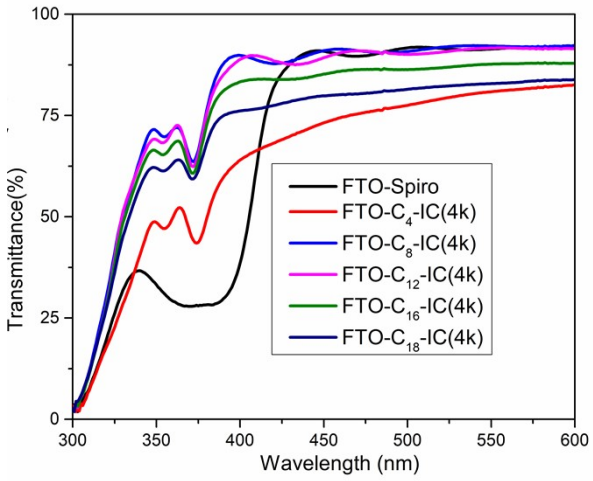

Figure S8. Transmittance spectra of *Spiro*-OMeTAD and C_RICs films over FTO.

4.11. Device parameter of PSC using C_RIC as HTMs

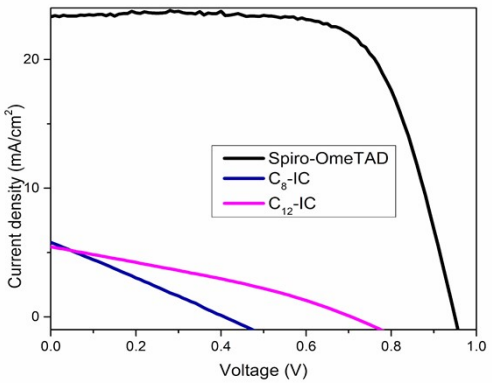

Figure S9. Backward J-V characteristics of doped *Spiro*-OMeTAD and undoped C_8IC and C_{12}IC.

Table S10. The parameters were extracted from the backward J-V characteristics of doped *Spiro*-OMeTAD and undoped C_8IC and C_{12}IC.

HTM	PCE (%)	Jsc (mA/cm^2)	Voc	FF
Spiro-OMeTAD (doped)	15.54	23.31	0.95	0.70
C_8IC (un-doped)	0.61	5.78	0.40	0.25
C_{12}IC (un-doped)	1.18	5.44	0.70	0.31

5. ^{1}H and ^{13}C NMR spectra of C_RIC HTMs

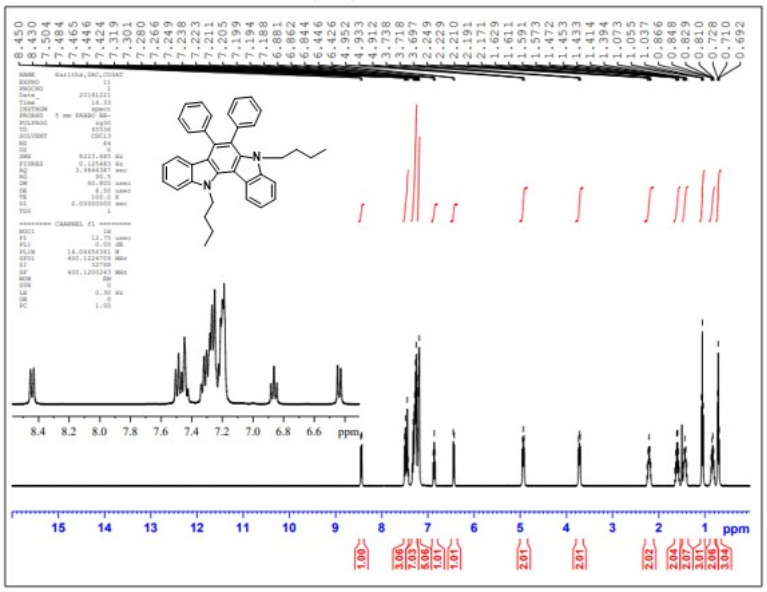

Figure S9. ^{1}H-NMR spectrum of **C_4IC** recorded in $CDCl_3$

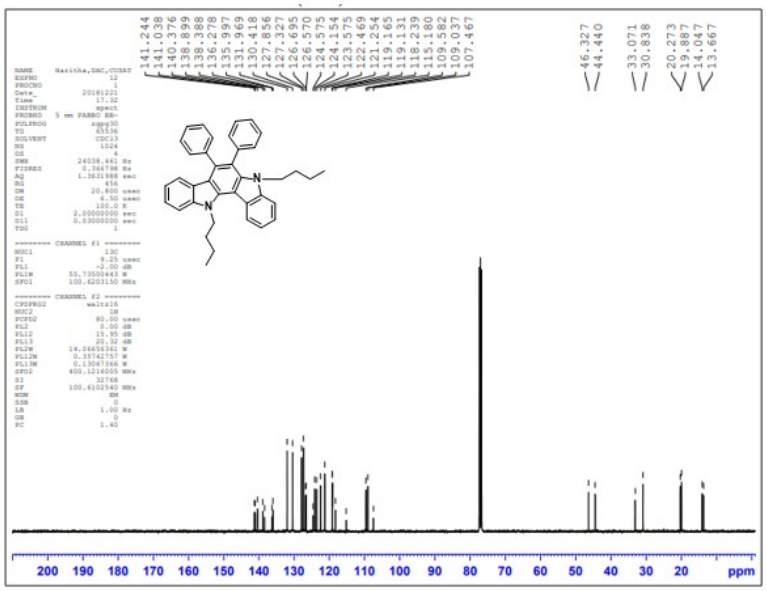

Figure S10. ^{13}C-NMR spectrum of **C_4IC** recorded in $CDCl_3$

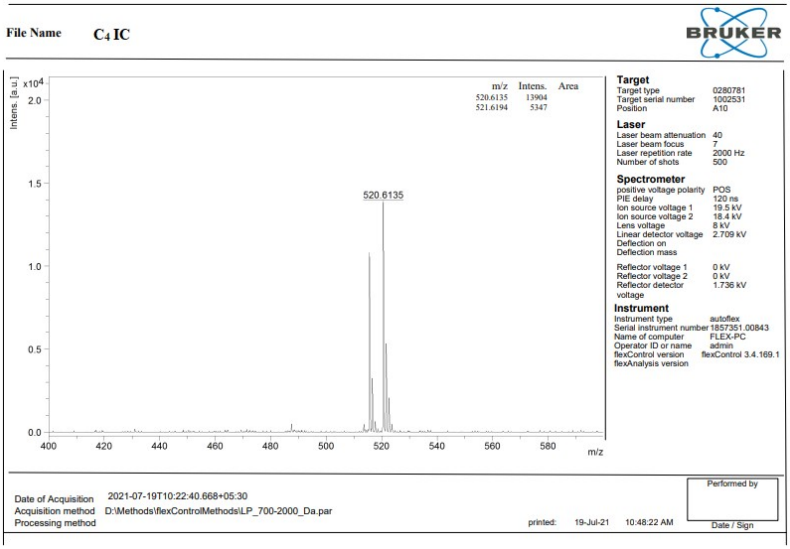

Figure S11. MALDI-TOF Spectrum of **C_4IC**

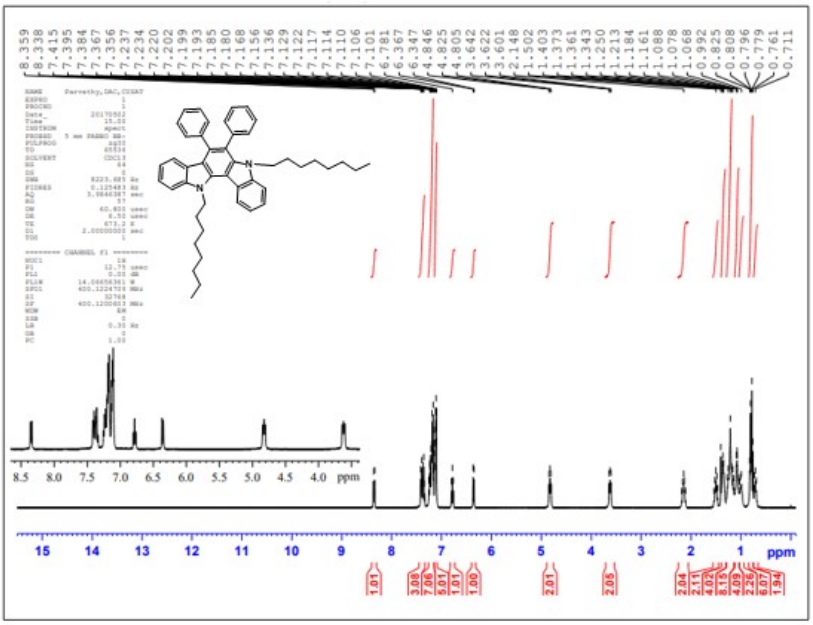

Figure S12. ^{1}H-NMR spectrum of **C_8IC** recorded in $CDCl_3$

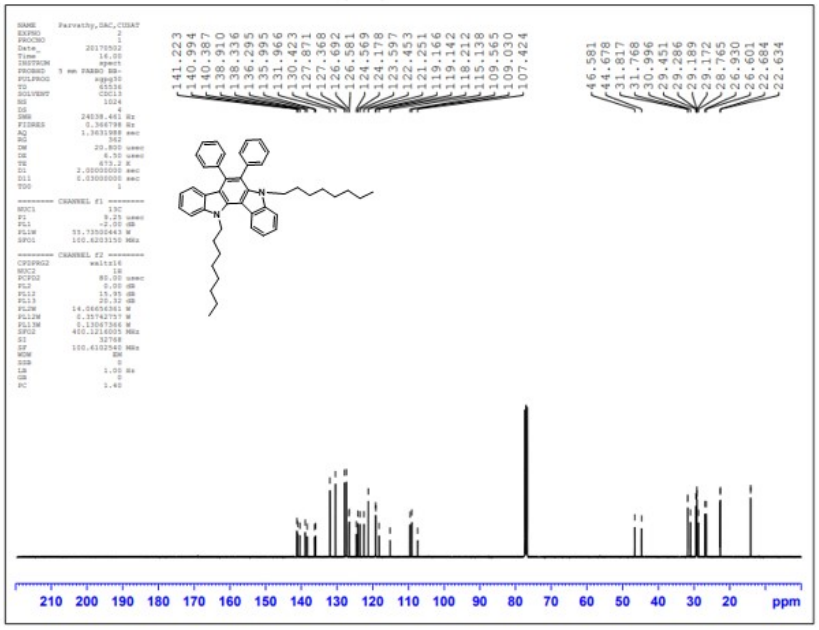

Figure S13. ^{13}C-NMR spectrum of **C_8IC** recorded in $CDCl_3$

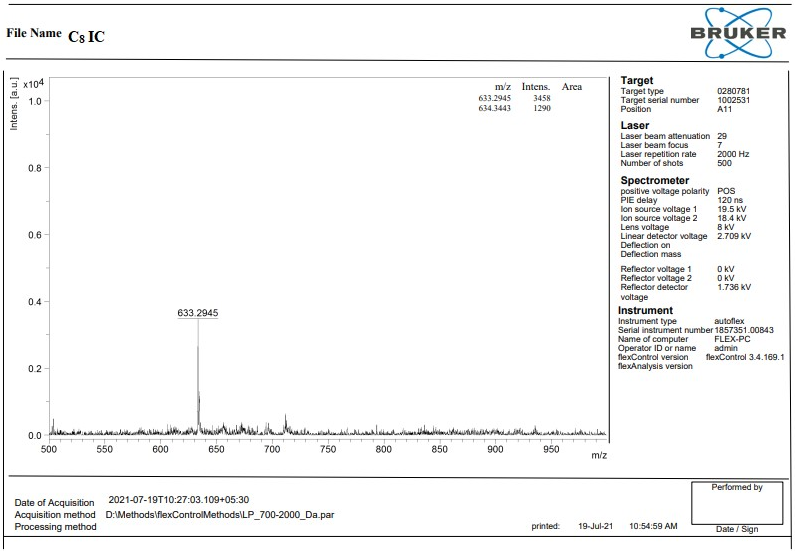

Figure S14. MALDI-TOF Spectrum of **C_8IC**

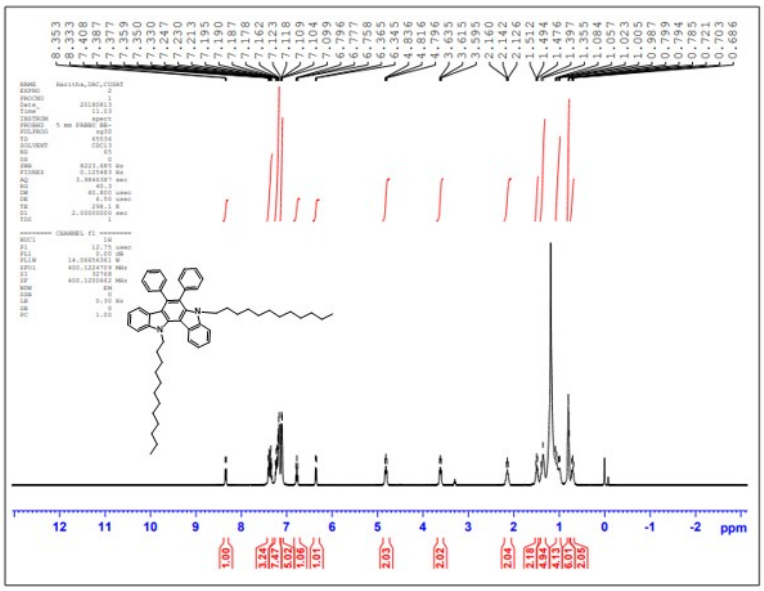

Figure S15. ^{1}H-NMR spectrum of **C_{12}IC** recorded in $CDCl_3$

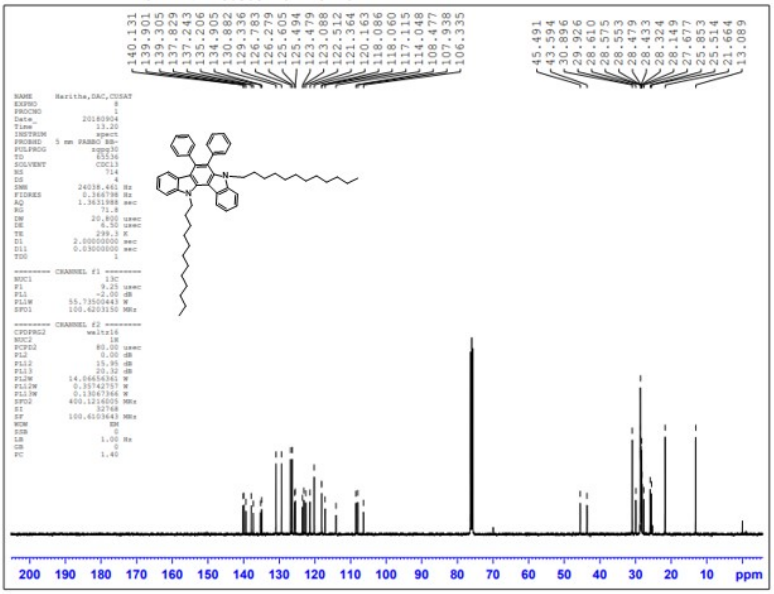

Figure S16. ^{13}C-NMR spectrum of **C_{12}IC** recorded in $CDCl_3$

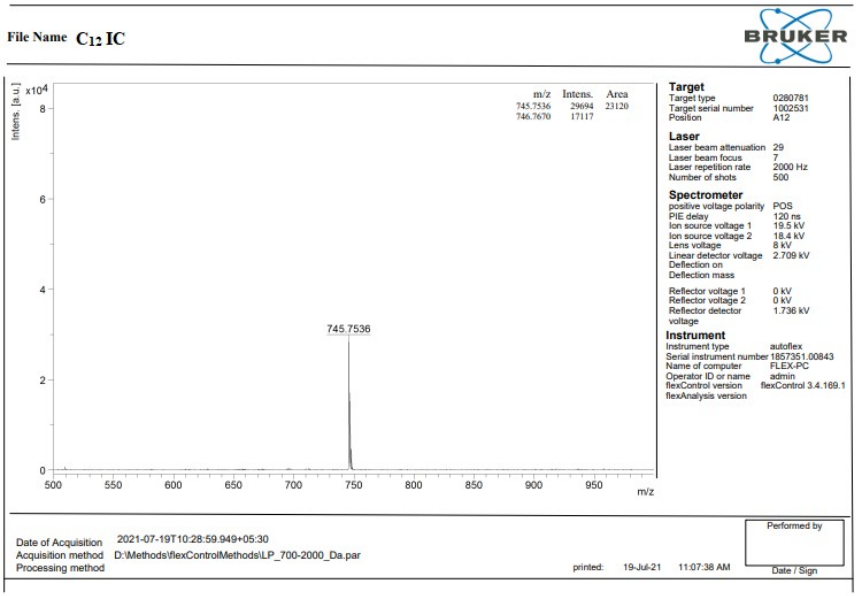

Figure S17. MALDI-TOF Spectrum of **C_{12}IC**

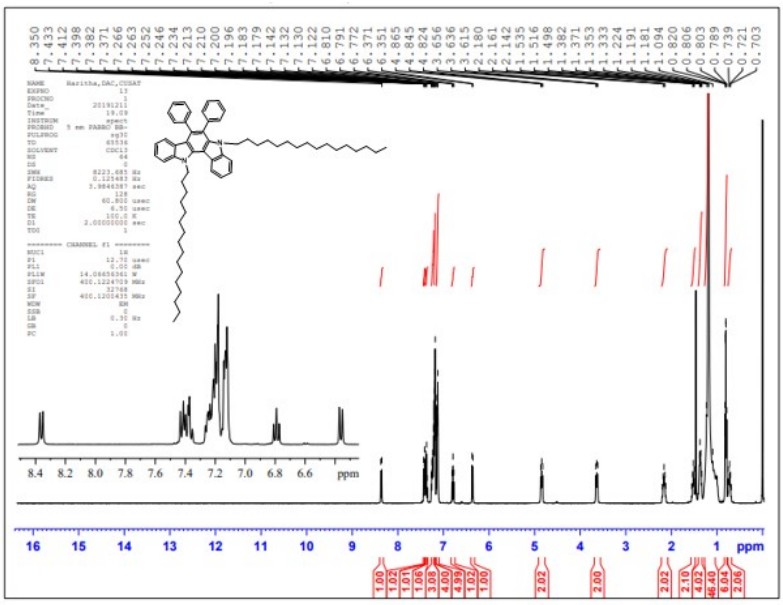

Figure S18. ^{1}H-NMR spectrum of **C_{16}IC** recorded in $CDCl_3$

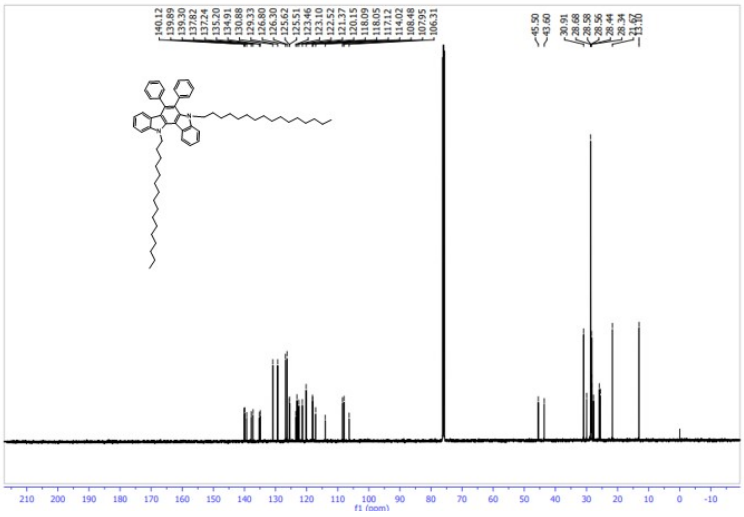

Figure S19. ^{13}C-NMR spectrum of **C_{16}IC** recorded in $CDCl_3$

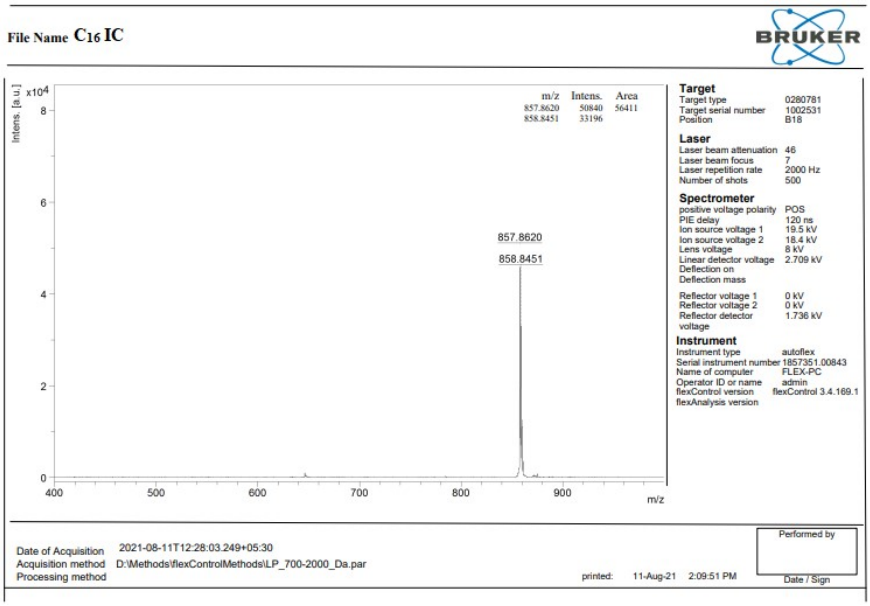

Figure S20. MALDI-TOF Spectrum of **C_{16}IC**

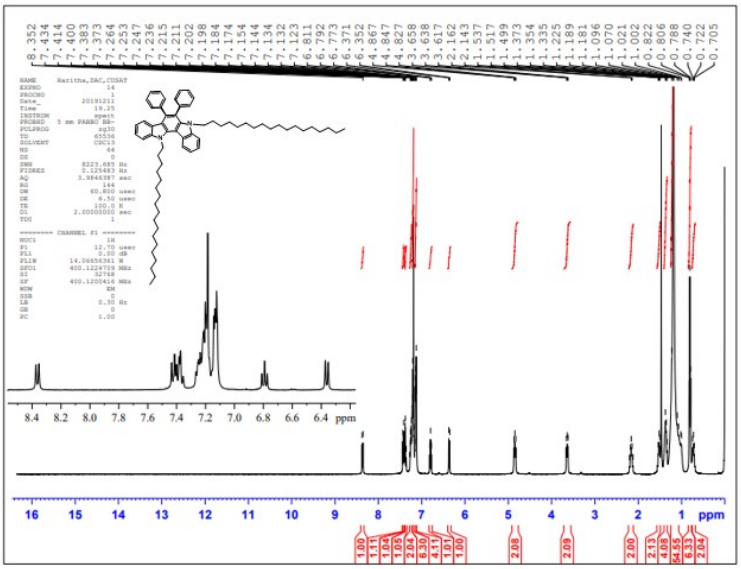

Figure S21. ^{1}H-NMR spectrum of **C_{18}IC** recorded in $CDCl_3$

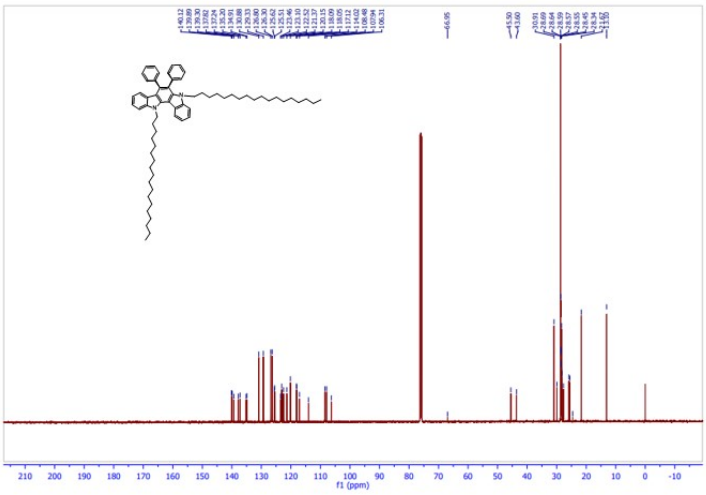

Figure S22. ^{13}C-NMR spectrum of **C_{18}IC** recorded in $CDCl_3$

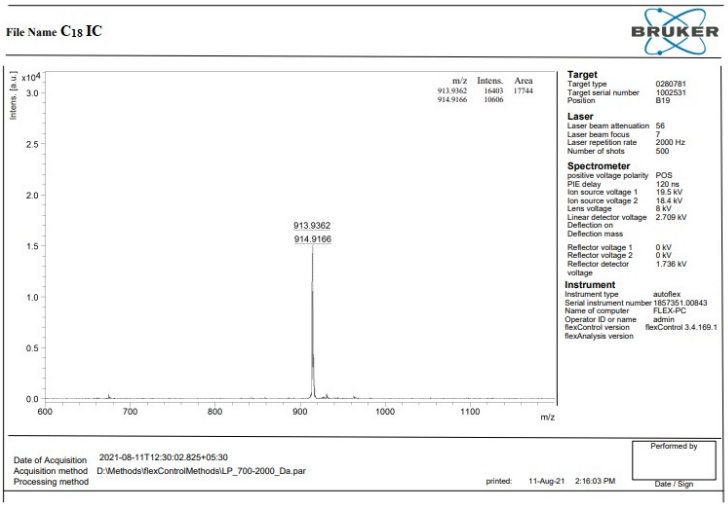

Figure S23. MALDI-TOF Spectrum of **C_{18}IC**

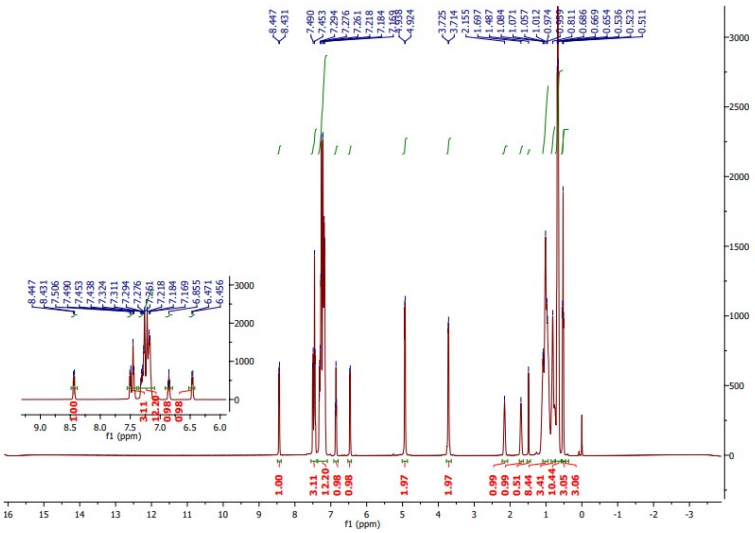

Figure S24. ^{1}H-NMR spectrum of **C_{ex}IC** recorded in $CDCl_3$

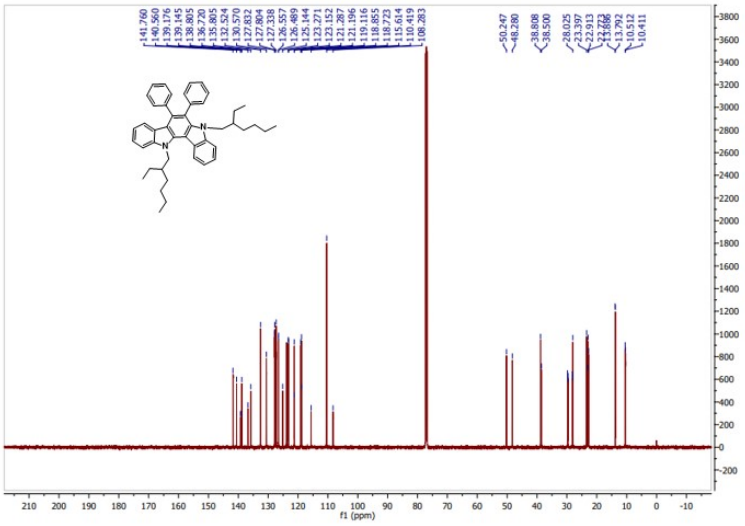

Figure S25. ^{13}C-NMR spectrum of **C_{ex}IC** recorded in $CDCl_3$

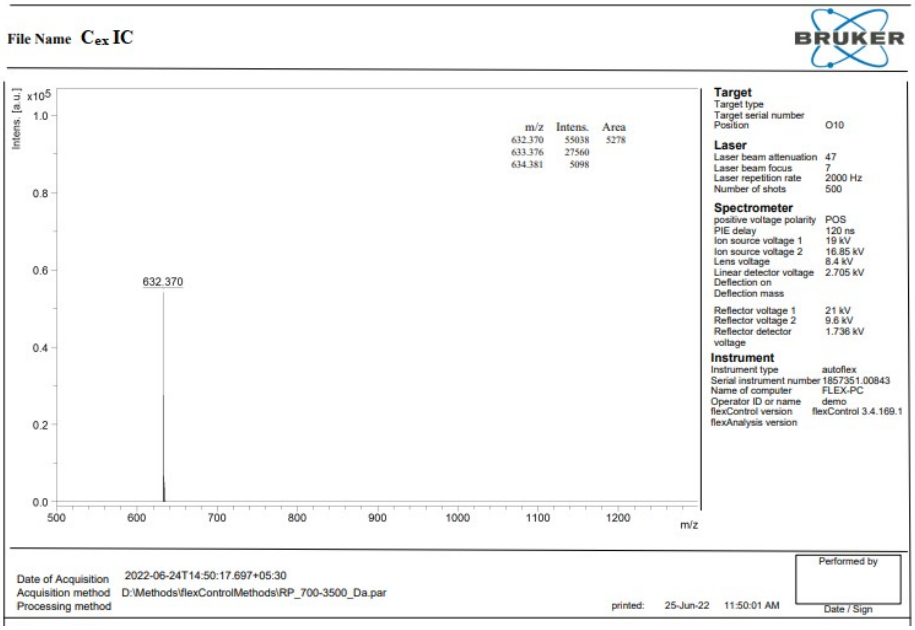

Figure S26. MALDI-TOF Spectrum of **C_{ex}IC**

6. Supporting Information References

1. V. Nair, V. Nandialath, K. G. Abhilash and E. Suresh, *Org. Biomol. Chem.*, 2008, **6**, 1738-1742.
2. K. S. Keremane, P. Naik and A. V. Adhikari, *J. Nano Electron. Phys.*, 2020, **12**, 02039.